analytical chemistry

Article

Spatial Metabolomics of the Human Kidney using MALDI Trapped Ion Mobility Imaging Mass Spectrometry

Elizabeth Kathleen Neumann, Lukasz G. Migas, Jamie L Allen, Richard M. Caprioli, Raf Van de Plas, and Jeffrey M. Spraggins

Anal. Chem., **Just Accepted Manuscript** • DOI: 10.1021/acs.analchem.0c02051 • Publication Date (Web): 15 Jul 2020

Spatial Metabolomics of the Human Kidney using MALDI Trapped Ion Mobility Imaging Mass Spectrometry

Elizabeth K. Neumann,[1,2] Lukasz G. Migas,[3] Jamie L. Allen,[2] Richard M. Caprioli,[1,2,4-6] Raf Van de Plas,[1-3] and Jeffrey M. Spraggins[1,2,6*]

[1]Department of Biochemistry, Vanderbilt University, 607 Light Hall, Nashville, TN 37205, USA

[2]Mass Spectrometry Research Center, Vanderbilt University, 465 21st Ave S #9160, Nashville, TN 37235, USA

[3]Delft Center for Systems and Control, Delft University of Technology, Mekelweg 2 Building 34, 2628 CD Delft, The Netherlands

[4]Department of Pharmacology, Vanderbilt University, 2220 Pierce Avenue, Nashville, TN 37232, USA

[5]Department of Medicine, Vanderbilt University, 465 21st Ave S #9160, Nashville, TN 37235, USA

[6]Department of Chemistry, Vanderbilt University, 7330 Stevenson Center, Station B 351822, Nashville, TN 37235, USA

KEYWORDS. Metabolomics, Human Kidney, Imaging mass spectrometry, Matrix-assisted laser desorption/ionization, Trapped ion mobility spectrometry, Ion mobility mass spectrometry, High spatial resolution imaging

ABSTRACT: Low molecular weight metabolites are essential for defining the molecular phenotypes of cells. However, spatial metabolomics tools often lack the sensitivity, specify, and spatial resolution to provide comprehensive descriptions of these species in tissue. MALDI imaging mass spectrometry (IMS) of low molecular weight ions is particularly challenging as MALDI matrix clusters are often nominally isobaric with multiple metabolite ions, requiring high resolving power instrumentation or derivatization to circumvent this issue. An alternative to this is to perform ion mobility separation before ion detection, enabling the visualization of metabolites without the interference of matrix ions. Additional difficulties surrounding low weight metabolite visualization include high resolution imaging, while maintaining sufficient ion numbers for broad and representative analysis of the tissue chemical complement. Here, we use MALDI timsTOF IMS to image low molecular weight metabolites at higher spatial resolution than most metabolite MALDI IMS experiments (20 μm) while maintaining broad coverage within the human kidney. We demonstrate that trapped ion mobility spectrometry (TIMS) can resolve matrix peaks from metabolite signal and separate both isobaric and isomeric metabolites with different distributions within the kidney. The added ion mobility data dimension dramatically increased the peak capacity for spatial metabolomics experiments. Through this improved sensitivity, we have found >40 low molecular weight metabolites in human kidney tissue such as arginic acid, acetylcarnitine, and choline that localize to the cortex, medulla, and renal pelvis, respectively. Future work will involve further exploring metabolomic profiles of human kidneys as a function of age, gender, and ethnicity.

Low molecular weight metabolites (< 600 Da) are essential for normal biological function and pathogenesis. The localization of these metabolites in tissue is important for cellular function and their disposition in disease may provide valuable insight into the (dis)functional state of human organs.[1] However, these small molecules are particularly difficult to analyze within tissue matrices because of their structural diversity and abundance of isomers.[2-3] Traditional means of exploring **low molecular weight** metabolites include capillary electrophoresis,[3-6] electrochemistry,[7-9] spectroscopy,[10-12] liquid chromatography,[13-15] and microscopy.[16-18] The discrete metabolites identified from each of these analyses have been integrated into databases, such as Metlin[19] and the Human Metabolome Database.[20] These analytical approaches have provided important insights into biological functions; however, they are often limited by throughput, specificity, sensitivity, or cannot be performed in an imaging regime.

Imaging mass spectrometry (IMS) is a powerful tool that enables untargeted, spatial analysis of hundreds of chemicals within a biological sample.[21] Matrix-assisted laser desorption/ionization (MALDI) IMS is a laser-based imaging technology used to study a variety of different chemical classes, ranging from metabolites, lipids, peptides, glycans, and proteins.[22-26] In summary, frozen tissue is typically cut on a cryostat into approximately 10 micron thick sections, thaw mounted onto a target, coated with an ultraviolet (UV) light-absorbing chemical matrix, and rastered under a UV laser.[24, 27] While exceptionally powerful for low molecular weight metabolite analysis,[28-31] the application of the organic matrix complicates small molecule analysis by MALDI IMS[32] because matrix ions are often nominally isobaric with low molecular weight metabolites.[33]

Several approaches exist for enhancing the detection of metabolites within a MALDI IMS experiment, generally by reducing matrix isobaric interferences. The most straightforward is to use high resolving power instruments, such as Fourier transform ion cyclotron resonance or Orbitrap mass spectrometers, to mass resolve the metabolites from matrix ions.[34-38] However, these systems cannot distinguish isomeric compounds without fragmentation and imaging times tend to be longer because of long scan times. Alternatively, other approaches have explored derivatization of the metabolites to enhance ionization and increase their respective mass-to-charge ratios (*m/z*), reducing isobaric interferences by matrix and other background ions.[39-46] Derivatization methods generally target specific functional groups and limit the number of different metabolite classes that can be simultaneously visualized. The derivatization step is often not quantitative and may also affect localization of soluble metabolites within tissue, resulting in altered spatial resolutions. Another approach is to utilize matrices that for specific analyses do not effectively interfere with the analysis of interest.[33,47] While effective, matrix choice can affect the types of molecules detected, so it is beneficial to develop methods compatible with a wide variety of matrices, particularly common matrices that have been extensively studied. By broadening metabolite analysis to include a variety of sampling approaches, we can extend the classes of low molecular weight metabolites that can be probed within a set of experiments rather than targeting a specific subset.

Ion mobility spectrometry is a gas phase analytical approach that enables the separation of ions based on their apparent size, shape, and charge state.[47-49] Specifically, trapped ion mobility spectrometry (TIMS) is a high resolution ion mobility technology that is compatible with imaging experiments and its time scales, unlike gas or liquid chromatography.[50] In brief, ions are initially trapped against an electric field while being pushed through the instrument by the flow of an inert gas. The magnitude of the electric field is progressively decreased, allowing the trapped ions to elute as a function of their mobility (*K*), which is dependent on the mass, charge, and size of the ion.[51-52] TIMS is capable of resolving powers greater than 250, enabling separation of lipid isomeric and isobaric species.[53] Other types of ion mobility spectrometry, such as traveling-wave[54-58] and drift tube[59], can discriminate and differentiate low molecular weight isomers as well but at lower ion mobility resolutions.

Here, we explore the metabolomic composition of the human kidney with MALDI trapped ion mobility IMS. Ultimately, we have achieved higher resolution than most metabolite experiments (20 µm), while maintaining enough sensitivity to detect >40 metabolites from a broad range of classes. Moreover, we have demonstrated that the use of TIMS enhances the discrimination and peak capacity of small molecule analysis within a quadrupole-time of flight (qTOF) MS, enabling high spatial resolution IMS analysis of low molecular weight metabolites (*m/z* 86-616) without significant interference from MALDI matrix ions. We also demonstrate that additional metabolite isomers and isobars can be visualized with ion mobility separations compared to qTOF only mode. As such, this technology enables imaging-based metabolomics with enhanced sensitivity and specificity at high spatial resolution.

METHODS

Materials:

α-Cyano-4-hydroxycinnamic acid (CHCA) was purchased from Sigma-Aldrich Chemical Co. (St. Louis, MO, USA). HPLC-grade acetonitrile, isopropanol, and methanol were purchased from Fisher Scientific (Pittsburgh, PA, USA).

Sample Preparation:

Human kidney tissue was surgically removed during a full nephrectomy and remnant tissue was processed for research purposes by the Cooperative Human Tissue Network at Vanderbilt University Medical Center. Remnant biospecimens were collected in compliance with the Cooperative Human Tissue Network standard protocols and National Cancer Institute's Best Practices for the procurement of remnant surgical research material. Participants were consented for remnant tissue collection in accordance to institutional IRB policies. The excised tissue was flash frozen over an isopentane, dry ice slurry, embedded in carboxymethylcellulose, and stored at -80 °C until use. Kidney tissues were cryosectioned to a 10 µm thickness and thaw mounted onto indium tin-oxide (ITO) coated glass slides (Delta Technologies, Loveland, CO, USA) and stored at -80 °C until analyzed. Tissues were returned to ~20 °C within a vacuum desiccator. Autofluorescence microscopy images were acquired using EGFP, DAPI and

DsRed filters on a Zeiss AxioScan Z1 slide scanner (Carl Zeiss Microscopy GmbH, Oberkochen, Germany) prior to matrix application.[60-61]. In total, tissue was wet at room temperature for >1 min.

Samples were coated with a 5 mg/mL solution of CHCA dissolved in a 70% methanol solution using an HTX TM Sprayer (HTX Technologies, LLC, Chapel Hill, NC, USA) yielding a 2.67 mg coating (1200 mm^2, 0.12 mL/hr, 8 passes, 4 sec drying time, 80 °C spray nozzle). Tissue samples were imaged immediately after matrix deposition and stored within a vacuum desiccator for subsequent tandem MS analysis.

MALDI timsTOF IMS:

MALDI TIMS IMS was performed on a prototype Bruker timsTOF fleX MS system[50] (Bruker Daltonics, Bremen, Germany) in both qTOF and TIMS analysis modes. Unless otherwise specified, qTOF ion images were collected in positive ion mode at 20 µm pixel size with the beam scan set to 18 $µm^2$ using 600 laser shots per pixel and 29% laser power (30% global attenuator and 99% local laser power) at 10 kHz. Data were collected from *m/z* 50 – 1500 for small metabolite analysis. Imaging data collected with TIMS activated were acquired at 20 µm pixel size with the beam scan set to 18 $µm^2$, 600 laser shots per pixel and 29% laser power (30% global attenuator and 99% local laser power) at 10 kHz. The TIMS electric field gradient scan time was set to 200 ms. Instrumental parameter metadata is provided in the supplementary materials and special tuning of the collision funnel RF values, TIMS ramp time, and TOF transfer time were required for metabolite imaging (SI Figure 1). A quadratic mass calibration and a linear ion mobility calibration were performed using reference mass lists of Agilent tune mix (Agilent Technologies, Santa Clara, CA). All qTOF mode imaging data were visualized using SCiLS Lab Version 2019 (Bruker Daltonics, Bremen, Germany) and TIMS imaging data were analyzed using custom in-house developed software. Metabolites were tentatively identified using mass accuracy to search the METLIN and Human Metabolome Databases, with assignment preference given to metabolites known to be found within the human kidney.. All putatively identified metabolites had mass accuracies of ≤ 4 ppm. Select ions were fragmented using tandem MS.

Data processing:

The kidney data was exported into a custom binary file format optimized for storage and speed of analysis of ion mobility-IMS data. Each individual frame contains between 10,000-100,000 centroid peaks that span the acquisition range of *m/z* 50-1500 and $1/K_0$ of 0.6-0.95 $Vscm^{-2}$ with 400,577 and 589 bins in the MS and ion mobility-dimensions, respectively. The processing pipeline requires common *m/z* and $1/K_0$ axes, hence individual centroid peaks were inserted at their correct bin position along the MS and IM-dimensions; missing values were set to zero. Following the conversion process, a mean mass spectrum of the entire dataset was retrieved and peak-picked. A total of ~500 most intense ions were then selected and examined to identify multi-conformational species, and they were visualised to examine conformation-specific ion localization in the spatial domain.

RESULTS AND DISCUSSION

Small Metabolite Analysis using MALDI timsTOF MS

We have developed a method for visualizing low molecular weight species (*m/z* 86-616) with MALDI ion mobility MS. In general, the detectability of metabolites is mostly dependent upon careful sample preparation to maintain metabolite localization, maximize signal intensity, and instrument tuning to transmit smaller *m/z* values. Sample preservation was performed as previously reported[62] with minimizing storage times, since many of these molecules are easily oxidized or are otherwise degraded. Kidney samples were immediately embedded in carboxymethyl cellulose, frozen at -80 °C until sectioned. The sectioned tissue was placed on an indium tin oxide glass slide and was coated with CHCA. Tissues were stored under vacuum before, during, and after analysis to reduce degradation. Overall, the imaging experiment was finished within a day of sectioning and later tandem MS occurred within a day or two post IMS. Moreover, several matrices and application parameters were examined to maximize analyte extraction without causing significant analyte delocalization (SI Table 1). High spatial resolution was achieved by applying matrix at a lower flow rate with additional passes from that reported in the literature[63], providing a drier matrix application. Finally, instrumental parameters must be optimized to transmit small molecules in addition to achieve high ion mobility resolving power. While careful tuning of each optic improves ion transmission, we found that the collision funnel RF values, TIMS ramp time, and TOF transfer time were most important in achieving optimal transmission of *m/z* values between 86 and 615 (SI Figure 1). Lowering the magnitude of the voltage applied to these optics increases the transmission of low molecular weight ions.

We have successfully detected >200 distinct species within the human kidney using qTOF-only mode and >350 discrete *m/z* values with TIMS separation enabled. The increase in the number of detectable ions by activating TIMS results from the accumulation of ions within the TIMS funnel prior to analysis. The detected ions were further separated into >900 features after incorporating the ion mobility dimension (Figure 1). The improved number of detected species after ion mobility separation demonstrates the effectiveness and power of MALDI TIMS for metabolite analysis. In total, we have detected different classes of metabolites, ranging from nutrients (pyridoxal, *m/z* 190.047) and food additives (2-acetylpyridine, *m/z* 144.044) to metabolism (n-methyltryptamine, *m/z* 197.105) and lipid precursors (choline, *m/z* 104.107), demonstrating the wide range of detectable ion classes with MALDI ion mobility IMS. Interestingly, there is a shift in detectable ions when TIMS is enabled, decreasing the number of ions detected below an *m/z* value of 150. Because the only instrumental parameters that were changed between qTOF mode and TIMS were those concerning ion mobility separation, this may indicate that lighter ions are lost during TIMS separations. Despite tuning each optic separately, the sensitivity of ions below an *m/z* value of 150 could not be readily reestablished, with some notable exceptions such as choline. Choline ions are likely detected because of their naturally high abundance within biological tissues.

In both qTOF and TIMS TOF modalities, the detectable features are difficult to identify due to their structural diversity and nondescript fragmentation profiles, commonly encountered for metabolite analysis. In these initial experiments, mass accuracy and a combination of Metlin and the Human Metabolome Databases were used to provisionally identify 46 of the detected ions (Table 1). While this is a fraction of the detected peaks, we only labeled peaks that had single peaks within the ion mobilogram as multiple peaks would indicate isomeric or isobaric features that are difficult to identify at this time. Additional features include isotopes, unknown species, and chemical noise. Future work will involve using standards to confirm the detected features and determine which isomers are resolved within the ion mobility dimension. The large number of detectable metabolites, particularly compared to what can be provisionally identified, demonstrates the necessity to further develop and improve untargeted metabolomic analyses. Further, as shown in Table 1, TIMS can detect metabolites from a variety of classes for untargeted spatial metabolomics.

High Spatial Resolution TIMS Imaging

The kidney is composed of a variety of structures (*e.g.* glomeruli and tubules) each contained in functional units within defined kidney regions. The cortex, medulla, and renal pelvis can be visualized by autofluorescence microscopy (Figure 2A) and is an excellent complement to IMS. IMS was performed at 20 μm pixel size and high signal-to-noise ratios (S/N) detection (Figure 2B-H). Many of the detectable metabolites are localized throughout the entire kidney, such as inosine (Figure 2 E&G), although several are detected within the different segments of the kidney. For example, choline and sapropterin are both detected in high abundance within the medulla and renal pelvis (Figure 2B&F), while acetylcarnitine is most abundant within the medulla (Figure 2D) and arginic acid is mostly detected within the cortex (Figure 2 C). Finally, heme is abundant in the kidney within blood vessels (Figure 2 H). While only a subset of detected molecules is displayed here, further examples of metabolites that localize to specific regions of the kidney can be found within the dataset (SI Figure 3). The function of many of these metabolites is well understood, such as lipid metabolism (choline),[64] fatty acid transport (acetylcarnitine)[65] and disordered urea metabolism (arginic acid).[66]

One of the most difficult challenges in spatial metabolomics is the unequivocal structural identification of a molecule. As seen by the number of ion mobility-resolved peaks, isobaric and isomeric compounds significantly complicate interpretation of imaging data and fragmentation experiments. We have performed fragmentation and subsequent identification of several of the detected small metabolites within the kidney (SI Figure 2). Diagnostic fragments for different metabolites at high S/N were generated by summing together spectra from the specific ion using different collision energies. Because spectra are obtained from a range of collision energies, each metabolite is more thoroughly characterized than if just by using a single collision energy. Many fragments, however, result in non-descript neutral losses (e.g. H2O and CO) rather than structurally identifying fragments (SI Figure 2). While not capable of providing absolute structural information, the

Measured *m/z* Value	Assignment	Mass Error (ppm)	$1/K_0$	Measured *m/z* Value	Assignment	Mass Error (ppm)	$1/K_0$
86.097	Choline-H_2O	-1.131	0.70	229.152	N-Decanoylglycine	-3.650	0.73
104.107	Choline	-0.394	0.71	232.151	Isobutyryl-carnitine	1.393	0.69
116.050	Mandelonitrile	-0.021	0.61	250.086	Gly-Ala-Cys	-0.198	0.77
144.044	2-Acetylpyridine	-1.190	0.62	251.982	M-Chlorohippuric acid	-0.028	0.77
146.981	Phosphonoacetaldehyde	0.589	0.64	258.107	Glycerophosphocholine	0.677	0.70
156.043	N-phenyl-Glycine	-0.779	0.73	275.146	Gln-Lys	3.936	0.80
166.061	4-Amino-2-Hydroxylamino-6-Nitrotoluene	-0.179	0.63	280.081	Sapropterin	-2.652	0.72
172.038	5,6-Dihydroxyindole	-0.466	0.61	285.004	Dihydrocaffeic Acid 3-Sulfate	-0.265	0.62
184.072	PC Head Group	0.935	0.65	307.044	Inosine	1.516	0.79
189.040	Methylisocitric acid	-0.336	0.62	311.074	Phlorin	-0.277	0.87
190.047	Pyridoxal (Vitamin B6)	-0.019	0.78	313.091	N2-Succinoylarginine	0.153	0.91
190.062	N-Methyltyramine	0.301	0.61	317.115	α-CEHC	-0.137	0.80
196.073	Pyroquilon	-0.008	0.60	346.041	5'-CMP	-0.384	0.85
197.105	N-Methyltryptamine	-0.041	0.60	355.101	Gly-Pro-Gly-Ser	0.181	0.89
198.088	Arginic Acid	-1.49	0.60	357.081	Asp-Gly-Ala-Gly	0.170	
200.972	N-Nitrosothiazolidine-4-Carboxylic Acid	0.433	0.67	373.054	His-Gly-OH	0.212	0.91
204.121	Acetylcarnitine	1.518	0.62	393.126	Met-Cys-Gly-Thr/Met-Cys-Ala-Ser	-0.105	0.91
206.054	Phosphocholine	0.773	0.64	427.079	5-Hydroxy-3,3',4',7,8-Pentamethoxyflavone	0.111	0.86
208.073	α-Naphthylacetamide	0.137	0.61	449.027	7,11,12-Triacetoxycoumestan	0.387	0.9
214.063	Baclofen	0.202	0.62	504.342	PC(O-16:0)	0.108	>1
215.083	3-(4-Isopropylphenyl)Propanal	0.359	0.61	534.292	Leu-Tyr-Lys-Glu	-0.182	>1
216.063	Betamipron	-0.086	0.65	616.197	Heme	3.305	>1

Table 1: Table of putatively identified (<5 ppm mass error) metabolites detected within the human kidney. While only one metabolite is shown here, we are likely detecting multiple isomers at each of these different *m/z* values.

profiles could be used to eliminate certain structures (e.g. loss of water indicates the presence of a hydroxyl group). As such, absolute identification of all detectable metabolites is relatively difficult and often does not aid in structural elucidation.

High-Performance Ion Mobility Separations of Small Molecules

The most cited limitation of MALDI analysis of metabolites in both a profiling and imaging context is the isobaric interference of matrix ions with key biological molecules.[67-70] While high resolving power instrumentation can resolve some of these nominally isobaric interferences, these analyses often require long scan times, leading to tradeoffs in either spatial resolution or the area imaged. However, high resolving power alone cannot discriminate isomeric species. The MALDI TIMS platform can be useful for this analysis and has been shown to discriminate isomeric species such as lipids within an LC experiment[53] and isobaric lipid species in an imaging experiment.[50]

We have utilized MALDI TIMS for the analysis of low molecular weight species and separation of isobaric matrix ions from endogenous metabolites (e.g. *m/z* 256.8, Figure 3). The composite image of a matrix ion and a metabolite ion (provisionally identified as glycerophosphocholine or GPC) shows high signal intensity off tissue and low intensity throughout the kidney tissue (Figure 3 inset). The extracted mobilogram of this *m/z* value shows two components, with the lower drift time associated with GPC (Figure 3B) and higher drift time associated with the matrix ion (Figure 3C). The detected distribution of the metabolite within the tissue is easier to discriminate within the ion mobility extracted image when compared to the composite image. Interestingly, the abundance of GPC is higher within the mobilogram than the matrix ion, despite having a lower intensity within the image. This is likely

due to the signal of GPC being distributed across more pixels than the matrix ion, so it is cumulatively higher in abundance than the matrix ion. GPC is one of the molecules used for lipid storage in tissue and is believed to protect renal cells from urea damage during normal kidney function. In this study, TIMS separated metabolites from MALDI generated chemical noise for over 30 *m/z* values, where matrix ions were isobaric to metabolite ions.

Ion mobility was used to separate isomeric and isobaric metabolomic features that show differential distribution within the kidney (Figure 4). In this example, the *m/z* value 267.956 separates into four different structures by ion mobility (Figure 4A), where the species with the lowest $1/K_0$ value localizes almost exclusively in the renal pelvis (Figure 4B) and the other three species are found in all three areas of the kidney (Figure 4C-E). The distribution of the fourth peak is lost almost entirely in the composite image (Figure 4A inset), demonstrating the information that can be gained from employing ion mobility separations to the low molecular weight mass range to improve sensitivity of low-abundant ions. The first three ion mobility-resolved peaks display very similar detected distributions within the kidney with only slight differences in ion abundances, perhaps indicating these are isomers or conformers, as opposed to isobars. Even if they are different conformers, it is still useful to probe how many conformers are present within a single *m/z* value as it could result from gas phase transitions or biologically-relevant differences. Future work will involve more complete identification of the ion mobility resolved peaks observed in human kidney tissue using standards.

In these examples, the addition of TIMS separations increases the amount of information that can be garnered from each pixel within the metabolite IMS experiment, both in terms of specificity and sensitivity. Practically, the image acquisition speed decreases due to the required TIMS scan time (60 ms per pixel here), which is faster than many high mass resolution experiments. Moreover, these metabolites were not derivatized and natively detected, enhancing the variety of detectable ions that can be simultaneously assessed compared to experiments that require the addition of a tag for metabolite analysis. Finally, the availability of TIMS may allow for a broader variety of matrices to be used for small metabolite analysis without interference, improving the types and extent of metabolite information that can be gained.

CONCLUSIONS

We have demonstrated that MALDI TIMS analysis can be applied to analyzing hundreds of low molecular weight metabolites within the human kidney. The combination of sample preparation, mass accuracy, and ion mobility separation presented here enables 20 µm visualization of small metabolites from a mixture of classes, such as nutrients, food additives, and metabolic biproducts. While not comprehensive of the metabolome, this marks a significant improvement to the field of spatial metabolomics. This platform improves the detectability of many ions by resolving metabolites from matrix ions and other metabolites in addition to accumulating ions prior to mass analysis. Moreover, TIMS drastically improves the applicability of MALDI IMS to metabolite analysis. Future work entails developing effective means of identification by incorporating standards and more comprehensive tandem MS analysis. MALDI ion mobility IMS has the capacity and propensity for allowing us to explore the metabolites responsible for key biological pathways and determine how metabolites change as a function of health and disease.

ASSOCIATED CONTENT

Supporting Information

The Supporting Information is available free of charge on the ACS Publications website.

AUTHOR INFORMATION

Corresponding Author

* Jeffery M. Spraggins, Jeff.Spraggins@vanderbilt.edu

Author Contributions

All authors have approved the final version of the manuscript.

ACKNOWLEDGMENTS

The authors would like to thank Maya Brewer and Prof. Mark deCaestecker for assistance and guidance with tissue processing and sample preparation. Support was provided by the NIH Common Fund and National Institute of Diabetes and Digestive and Kidney Diseases (U54DK120058 awarded to J.M.S. and R.M.C.), NIH National Institute of Allergy and Infectious Disease (R01 AI138581 awarded to J.M.S.), the National Science Foundation Major Research Instrument Program (CBET – 1828299 awarded to J.M.S. and R.M.C.)., and by the NIH National Institute of General Medical Sciences (2P41GM103391 awarded to R.M.C.). E.K.N. is supported by a National Institute of Environmental Health Sciences training grant (T32ES007028). The Cooperative Human Tissue Network is supported by the NIH National Cancer Institute (5 UM1 CA183727-08).

REFERENCES

1. Weiss, R. H.; Kim, K. Metabolomics in the study of kidney diseases *Nature Reviews Nephrology* **2012,** *8* (1), 22-33.
2. Dettmer, K.; Aronov, P. A.; Hammock, B. D. Mass spectrometry-based metabolomics *Mass Spectrometry Reviews* **2007,** *26* (1), 51-78.
3. Monton, M. R. N.; Soga, T. Metabolome analysis by capillary electrophoresis–mass spectrometry *Journal of Chromatography A* **2007,** *1168* (1), 237-246.
4. Soga, T.; Ohashi, Y.; Ueno, Y.; Naraoka, H.; Tomita, M.; Nishioka, T. Quantitative Metabolome Analysis Using Capillary Electrophoresis Mass Spectrometry *Journal of Proteome Research* **2003,** *2* (5), 488-494.
5. Hirayama, A.; Kami, K.; Sugimoto, M.; Sugawara, M.; Toki, N.; Onozuka, H.; Kinoshita, T.; Saito, N.; Ochiai, A.; Tomita, M.; Esumi, H.; Soga, T. Quantitative Metabolome Profiling of Colon and Stomach Cancer Microenvironment by Capillary Electrophoresis Time-of-Flight Mass Spectrometry *Cancer Research* **2009,** *69* (11), 4918-4925.
6. Ramautar, R.; Demirci, A.; Jong, G. J. d. Capillary electrophoresis in metabolomics *TrAC Trends in Analytical Chemistry* **2006,** *25* (5), 455-466.
7. Gamache, P. H.; Meyer, D. F.; Granger, M. C.; Acworth, I. N. Metabolomic applications of electrochemistry/Mass spectrometry *Journal of the American Society for Mass Spectrometry* **2004,** *15* (12), 1717-1726.
8. Bogdanov, M.; Matson, W. R.; Wang, L.; Matson, T.; Saunders-Pullman, R.; Bressman, S. S.; Beal, M. F. Metabolomic profiling to develop blood biomarkers for Parkinson's disease *Brain* **2008,** *131* (2), 389-396.

9. Kaddurah-Daouk, R.; Yuan, P.; Boyle, S. H.; Matson, W.; Wang, Z.; Zeng, Z. B.; Zhu, H.; Dougherty, G. G.; Yao, J. K.; Chen, G.; Guitart, X.; Carlson, P. J.; Neumeister, A.; Zarate, C.; Krishnan, R. R.; Manji, H. K.; Drevets, W. Cerebrospinal Fluid Metabolome in Mood Disorders-Remission State has a Unique Metabolic Profile *Scientific Reports* **2012,** *2* (1), 667.

10. Pan, Z.; Raftery, D. Comparing and combining NMR spectroscopy and mass spectrometry in metabolomics *Analytical and Bioanalytical Chemistry* **2007,** *387* (2), 525-527.

11. Beckonert, O.; Keun, H. C.; Ebbels, T. M. D.; Bundy, J.; Holmes, E.; Lindon, J. C.; Nicholson, J. K. Metabolic profiling, metabolomic and metabonomic procedures for NMR spectroscopy of urine, plasma, serum and tissue extracts *Nature Protocols* **2007,** *2* (11), 2692-2703.

12. Ward, J. L.; Baker, J. M.; Beale, M. H. Recent applications of NMR spectroscopy in plant metabolomics *The FEBS Journal* **2007,** *274* (5), 1126-1131.

13. Moco, S.; Bino, R. J.; Vorst, O.; Verhoeven, H. A.; de Groot, J.; van Beek, T. A.; Vervoort, J.; de Vos, C. H. R. A Liquid Chromatography-Mass Spectrometry-Based Metabolome Database for Tomato *Plant Physiology* **2006,** *141* (4), 1205-1218.

14. De Vos, R. C. H.; Moco, S.; Lommen, A.; Keurentjes, J. J. B.; Bino, R. J.; Hall, R. D. Untargeted large-scale plant metabolomics using liquid chromatography coupled to mass spectrometry *Nature Protocols* **2007,** *2* (4), 778-791.

15. Gika, H. G.; Theodoridis, G. A.; Plumb, R. S.; Wilson, I. D. Current practice of liquid chromatography–mass spectrometry in metabolomics and metabonomics *Journal of Pharmaceutical and Biomedical Analysis* **2014,** *87*, 12-25.

16. Fessenden, M. Metabolomics: Small molecules, single cells *Nature* **2016,** *540* (7631), 153-155.

17. Yaseen, M. A.; Sakadžić, S.; Wu, W.; Becker, W.; Kasischke, K. A.; Boas, D. A. In vivo imaging of cerebral energy metabolism with two-photon fluorescence lifetime microscopy of NADH *Biomed. Opt. Express* **2013,** *4* (2), 307-321.

18. Piston, D. W.; Knobel, S. M. Real-time Analysis of Glucose Metabolism by Microscopy *Trends in Endocrinology & Metabolism* **1999,** *10* (10), 413-417.

19. Guijas, C.; Montenegro-Burke, J. R.; Domingo-Almenara, X.; Palermo, A.; Warth, B.; Hermann, G.; Koellensperger, G.; Huan, T.; Uritboonthai, W.; Aisporna, A. E.; Wolan, D. W.; Spilker, M. E.; Benton, H. P.; Siuzdak, G. METLIN: A Technology Platform for Identifying Knowns and Unknowns *Analytical Chemistry* **2018,** *90* (5), 3156-3164.

20. Wishart, D. S.; Tzur, D.; Knox, C.; Eisner, R.; Guo, A. C.; Young, N.; Cheng, D.; Jewell, K.; Arndt, D.; Sawhney, S.; Fung, C.; Nikolai, L.; Lewis, M.; Coutouly, M.-A.; Forsythe, I.; Tang, P.; Shrivastava, S.; Jeroncic, K.; Stothard, P.; Amegbey, G.; Block, D.; Hau, D. D.; Wagner, J.; Miniaci, J.; Clements, M.; Gebremedhin, M.; Guo, N.; Zhang, Y.; Duggan, G. E.; MacInnis, G. D.; Weljie, A. M.; Dowlatabadi, R.; Bamforth, F.; Clive, D.; Greiner, R.; Li, L.; Marrie, T.; Sykes, B. D.; Vogel, H. J.; Querengesser, L. HMDB: the Human Metabolome Database *Nucleic Acids Research* **2007,** *35* (suppl_1), D521-D526.

21. Caprioli, R. M.; Farmer, T. B.; Gile, J. Molecular Imaging of Biological Samples: Localization of Peptides and Proteins Using MALDI-TOF MS *Analytical Chemistry* **1997,** *69* (23), 4751-4760.

22. McDonnell, L. A.; Heeren, R. M. A. Imaging mass spectrometry *Mass Spectrometry Reviews* **2007,** *26* (4), 606-643.

23. Amstalden van Hove, E. R.; Smith, D. F.; Heeren, R. M. A. A concise review of mass spectrometry imaging *Journal of Chromatography A* **2010,** *1217* (25), 3946-3954.

24. Neumann, E. K.; Do, T. D.; Comi, T. J.; Sweedler, J. V. Exploring the Fundamental Structures of Life: Non-Targeted, Chemical Analysis of Single Cells and Subcellular Structures *Angewandte Chemie International Edition* **2019,** *58* (28), 9348-9364.

25. Xu, X.; Zhong, J.; Su, Y.; Zou, Z.; He, Y.; Hou, X. A brief review on mass/optical spectrometry for imaging analysis of biological samples *Applied Spectroscopy Reviews* **2019,** *54* (1), 57-85.

26. Zemski Berry, K. A.; Hankin, J. A.; Barkley, R. M.; Spraggins, J. M.; Caprioli, R. M.; Murphy, R. C. MALDI Imaging of Lipid Biochemistry in Tissues by Mass Spectrometry *Chemical Reviews* **2011,** *111* (10), 6491-6512.

27. El-Aneed, A.; Cohen, A.; Banoub, J. Mass Spectrometry, Review of the Basics: Electrospray, MALDI, and Commonly Used Mass Analyzers *Applied Spectroscopy Reviews* **2009,** *44* (3), 210-230.

28. Cohen, L. H.; Gusev, A. I. Small molecule analysis by MALDI mass spectrometry *Analytical and Bioanalytical Chemistry* **2002,** *373* (7), 571-586.

29. Shrivas, K.; Hayasaka, T.; Sugiura, Y.; Setou, M. Method for Simultaneous Imaging of Endogenous Low Molecular Weight Metabolites in Mouse Brain Using TiO2 Nanoparticles in Nanoparticle-Assisted Laser Desorption/Ionization-Imaging Mass Spectrometry *Analytical Chemistry* **2011,** *83* (19), 7283-7289.

30. Nemes, P.; Woods, A. S.; Vertes, A. Simultaneous Imaging of Small Metabolites and Lipids in Rat Brain Tissues at Atmospheric Pressure by Laser Ablation Electrospray Ionization Mass Spectrometry *Analytical Chemistry* **2010,** *82* (3), 982-988.

31. Jiang, S.; Liang, Z.; Hao, L.; Li, L. Investigation of signaling molecules and metabolites found in crustacean hemolymph via in vivo microdialysis using a multifaceted mass spectrometric platform *ELECTROPHORESIS* **2016,** *37* (7-8), 1031-1038.

32. Calvano, C. D.; Monopoli, A.; Cataldi, T. R. I.; Palmisano, F. MALDI matrices for low molecular weight compounds: an endless story? *Analytical and Bioanalytical Chemistry* **2018,** *410* (17), 4015-4038.

33. Shanta, S. R.; Kim, T. Y.; Hong, J. H.; Lee, J. H.; Shin, C. Y.; Kim, K.-H.; Kim, Y. H.; Kim, S. K.; Kim, K. P. A new combination MALDI matrix for small molecule analysis: application to imaging mass spectrometry for drugs and metabolites *Analyst* **2012,** *137* (24), 5757-5762.

34. Buck, A.; Ly, A.; Balluff, B.; Sun, N.; Gorzolka, K.; Feuchtinger, A.; Janssen, K.-P.; Kuppen, P. J.; van de Velde, C. J.; Weirich, G.; Erlmeier, F.; Langer, R.; Aubele, M.; Zitzelsberger, H.; Aichler, M.; Walch, A. High-resolution MALDI-FT-ICR MS imaging for the analysis of metabolites from formalin-fixed, paraffin-embedded clinical tissue samples *The Journal of Pathology* **2015,** *237* (1), 123-132.

35. Kunzke, T.; Buck, A.; Prade, V. M.; Feuchtinger, A.; Prokopchuk, O.; Martignoni, M. E.; Heisz, S.; Hauner, H.; Janssen, K.-P.; Walch, A.; Aichler, M. Derangements of amino acids in cachectic skeletal muscle are caused by mitochondrial dysfunction *Journal of Cachexia, Sarcopenia and Muscle n/a* (n/a).

36. Barry, J. A.; Groseclose, M. R.; Robichaud, G.; Castellino, S.; Muddiman, D. C. Assessing drug and metabolite detection in liver tissue by UV-MALDI and IR-MALDESI mass spectrometry imaging coupled to FT-ICR MS *International Journal of Mass Spectrometry* **2015,** *377*, 448-455.

37. Buck, A.; Halbritter, S.; Späth, C.; Feuchtinger, A.; Aichler, M.; Zitzelsberger, H.; Janssen, K.-P.; Walch, A. Distribution and quantification of irinotecan and its active metabolite SN-38 in colon cancer murine model systems using MALDI MSI *Analytical and Bioanalytical Chemistry* **2015,** *407* (8), 2107-2116.

38. Wang, H.-Y.; Chu, X.; Zhao, Z.-X.; He, X.-S.; Guo, Y.-L. Analysis of low molecular weight compounds by MALDI-FTICR-MS *Journal of Chromatography B* **2011,** *879* (17), 1166-1179.

39. Wu, Q.; Comi, T. J.; Li, B.; Rubakhin, S. S.; Sweedler, J. V. On-Tissue Derivatization via Electrospray Deposition for Matrix-Assisted Laser Desorption/Ionization Mass Spectrometry Imaging of Endogenous Fatty Acids in Rat Brain Tissues *Analytical Chemistry* **2016,** *88* (11), 5988-5995.

40. Zaikin, V. G.; Halket, J. M. Derivatization in Mass Spectrometry—8. Soft Ionization Mass Spectrometry of Small Molecules *European Journal of Mass Spectrometry* **2006,** *12* (2), 79-115.

41. Tholey, A.; Wittmann, C.; Kang, M.-J.; Bungert, D.; Hollemeyer, K.; Heinzle, E. Derivatization of small biomolecules for optimized matrix-assisted laser desorption/ionization mass spectrometry *Journal of Mass Spectrometry* **2002,** *37* (9), 963-973.

42. Toue, S.; Sugiura, Y.; Kubo, A.; Ohmura, M.; Karakawa, S.; Mizukoshi, T.; Yoneda, J.; Miyano, H.; Noguchi, Y.; Kobayashi, T.; Kabe, Y.; Suematsu, M. Microscopic imaging mass spectrometry assisted by on-tissue chemical derivatization for visualizing multiple amino acids in human colon cancer xenografts *PROTEOMICS* **2014,** *14* (7-8), 810-819.

43. Esteve, C.; Tolner, E. A.; Shyti, R.; van den Maagdenberg, A. M. J. M.; McDonnell, L. A. Mass spectrometry imaging of amino neurotransmitters: a comparison of derivatization methods and application in mouse brain tissue *Metabolomics* **2016,** *12* (2), 30.

44. Chacon, A.; Zagol-Ikapitte, I.; Amarnath, V.; Reyzer, M. L.; Oates, J. A.; Caprioli, R. M.; Boutaud, O. On-tissue chemical derivatization

of 3-methoxysalicylamine for MALDI-imaging mass spectrometry *Journal of Mass Spectrometry* **2011,** *46* (8), 840-846.

45. Manier, M. L.; Spraggins, J. M.; Reyzer, M. L.; Norris, J. L.; Caprioli, R. M. A derivatization and validation strategy for determining the spatial localization of endogenous amine metabolites in tissues using MALDI imaging mass spectrometry *Journal of Mass Spectrometry* **2014,** *49* (8), 665-673.

46. Shariatgorji, M.; Nilsson, A.; Fridjonsdottir, E.; Vallianatou, T.; Källback, P.; Katan, L.; Sävmarker, J.; Mantas, I.; Zhang, X.; Bezard, E.; Svenningsson, P.; Odell, L. R.; Andrén, P. E. Comprehensive mapping of neurotransmitter networks by MALDI–MS imaging *Nature Methods* **2019,** *16* (10), 1021-1028.

47. Burnum-Johnson, K. E.; Zheng, X.; Dodds, J. N.; Ash, J.; Fourches, D.; Nicora, C. D.; Wendler, J. P.; Metz, T. O.; Waters, K. M.; Jansson, J. K.; Smith, R. D.; Baker, E. S. Ion mobility spectrometry and the omics: Distinguishing isomers, molecular classes and contaminant ions in complex samples *TrAC Trends in Analytical Chemistry* **2019,** *116*, 292-299.

48. Zhang, X.; Quinn, K.; Cruickshank-Quinn, C.; Reisdorph, R.; Reisdorph, N. The application of ion mobility mass spectrometry to metabolomics *Current Opinion in Chemical Biology* **2018,** *42*, 60-66.

49. Dodds, J. N.; Baker, E. S. Ion Mobility Spectrometry: Fundamental Concepts, Instrumentation, Applications, and the Road Ahead *Journal of the American Society for Mass Spectrometry* **2019,** *30* (11), 2185-2195.

50. Spraggins, J. M.; Djambazova, K. V.; Rivera, E. S.; Migas, L. G.; Neumann, E. K.; Fuetterer, A.; Suetering, J.; Goedecke, N.; Ly, A.; Van de Plas, R.; Caprioli, R. M. High-Performance Molecular Imaging with MALDI Trapped Ion-Mobility Time-of-Flight (timsTOF) Mass Spectrometry *Analytical Chemistry* **2019,** *91* (22), 14552-14560.

51. Ridgeway, M. E.; Lubeck, M.; Jordens, J.; Mann, M.; Park, M. A. Trapped ion mobility spectrometry: A short review *International Journal of Mass Spectrometry* **2018,** *425*, 22-35.

52. Silveira, J. A.; Michelmann, K.; Ridgeway, M. E.; Park, M. A. Fundamentals of Trapped Ion Mobility Spectrometry Part II: Fluid Dynamics *Journal of the American Society for Mass Spectrometry* **2016,** *27* (4), 585-595.

53. Jeanne Dit Fouque, K.; Ramirez, C. E.; Lewis, R. L.; Koelmel, J. P.; Garrett, T. J.; Yost, R. A.; Fernandez-Lima, F. Effective Liquid Chromatography–Trapped Ion Mobility Spectrometry–Mass Spectrometry Separation of Isomeric Lipid Species *Analytical Chemistry* **2019,** *91* (8), 5021-5027.

54. Paglia, G.; Astarita, G. Metabolomics and lipidomics using traveling-wave ion mobility mass spectrometry *Nature Protocols* **2017,** *12* (4), 797-813.

55. Zhang, L.; Allworth, L. L.; Vertes, A., In *Single Cell Metabolism: Methods and Protocols*, Shrestha, B., Ed. Springer New York: New York, NY, 2020; pp 9-18.

56. Chughtai, K.; Jiang, L.; Greenwood, T. R.; Glunde, K.; Heeren, R. M. A. Mass spectrometry images acylcarnitines, phosphatidylcholines, and sphingomyelin in MDA-MB-231 breast tumor models *Journal of Lipid Research* **2013,** *54* (2), 333-344.

57. Blatherwick, E. Q.; Svensson, C. I.; Frenguelli, B. G.; Scrivens, J. H. Localisation of adenine nucleotides in heat-stabilised mouse brains using ion mobility enabled MALDI imaging *International Journal of Mass Spectrometry* **2013,** *345-347*, 19-27.

58. Li, H.; Smith, B. K.; Márk, L.; Nemes, P.; Nazarian, J.; Vertes, A. Ambient molecular imaging by laser ablation electrospray ionization mass spectrometry with ion mobility separation *International Journal of Mass Spectrometry* **2015,** *377*, 681-689.

59. Zheng, X.; Aly, N. A.; Zhou, Y.; Dupuis, K. T.; Bilbao, A.; Paurus, Vanessa L.; Orton, D. J.; Wilson, R.; Payne, S. H.; Smith, R. D.; Baker, E. S. A structural examination and collision cross section database for over 500 metabolites and xenobiotics using drift tube ion mobility spectrometry *Chemical Science* **2017,** *8* (11), 7724-7736.

60. Patterson, N. H.; Tuck, M.; Lewis, A.; Kaushansky, A.; Norris, J. L.; Van de Plas, R.; Caprioli, R. M. Next Generation Histology-Directed Imaging Mass Spectrometry Driven by Autofluorescence Microscopy *Analytical Chemistry* **2018,** *90* (21), 12404-12413.

61. Patterson, N. H.; Tuck, M.; Van de Plas, R.; Caprioli, R. M. Advanced Registration and Analysis of MALDI Imaging Mass Spectrometry Measurements through Autofluorescence Microscopy *Analytical Chemistry* **2018,** *90* (21), 12395-12403.

62. Goodwin, R. J. A. Sample preparation for mass spectrometry imaging: Small mistakes can lead to big consequences *Journal of Proteomics* **2012,** *75* (16), 4893-4911.

63. Gemperline, E.; Rawson, S.; Li, L. Optimization and Comparison of Multiple MALDI Matrix Application Methods for Small Molecule Mass Spectrometric Imaging *Analytical Chemistry* **2014,** *86* (20), 10030-10035.

64. Synoradzki, K.; Grieb, P. Citicoline: A Superior Form of Choline? *Nutrients* **2019,** *11* (7), 1569.

65. Roseiro, L. C.; Santos, C., In *Nonvitamin and Nonmineral Nutritional Supplements*, Nabavi, S. M.; Silva, A. S., Eds. Academic Press: 2019; pp 45-52.

66. Vanholder, R.; De Smet, R.; Glorieux, G.; Argilés, A.; Baurmeister, U.; Brunet, P.; Clark, W.; Cohen, G.; De Deyn, P. P.; Deppisch, R.; Descamps-Latscha, B.; Henle, T.; Jörres, A.; Lemke, H. D.; Massy, Z. A.; Passlick-Deetjen, J.; Rodriguez, M.; Stegmayr, B.; Stenvinkel, P.; Tetta, C.; Wanner, C.; Zidek, W.; For the European Uremic Toxin Work, G. Review on uremic toxins: Classification, concentration, and interindividual variability *Kidney International* **2003,** *63* (5), 1934-1943.

67. Sugiura, Y.; Setou, M. Imaging Mass Spectrometry for Visualization of Drug and Endogenous Metabolite Distribution: Toward In Situ Pharmacometabolomes *Journal of Neuroimmune Pharmacology* **2010,** *5* (1), 31-43.

68. Castellino, S.; Groseclose, M. R.; Wagner, D. MALDI imaging mass spectrometry: bridging biology and chemistry in drug development *Bioanalysis* **2011,** *3* (21), 2427-2441.

69. Lietz, C. B.; Gemperline, E.; Li, L. Qualitative and quantitative mass spectrometry imaging of drugs and metabolites *Advanced Drug Delivery Reviews* **2013,** *65* (8), 1074-1085.

70. Greer, T.; Sturm, R.; Li, L. Mass spectrometry imaging for drugs and metabolites *Journal of Proteomics* **2011,** *74* (12), 2617-2631.

TOC

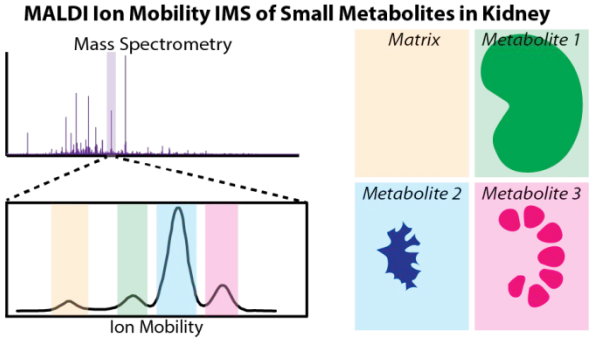
MALDI Ion Mobility IMS of Small Metabolites in Kidney
Mass Spectrometry
Ion Mobility
Matrix
Metabolite 1
Metabolite 2
Metabolite 3

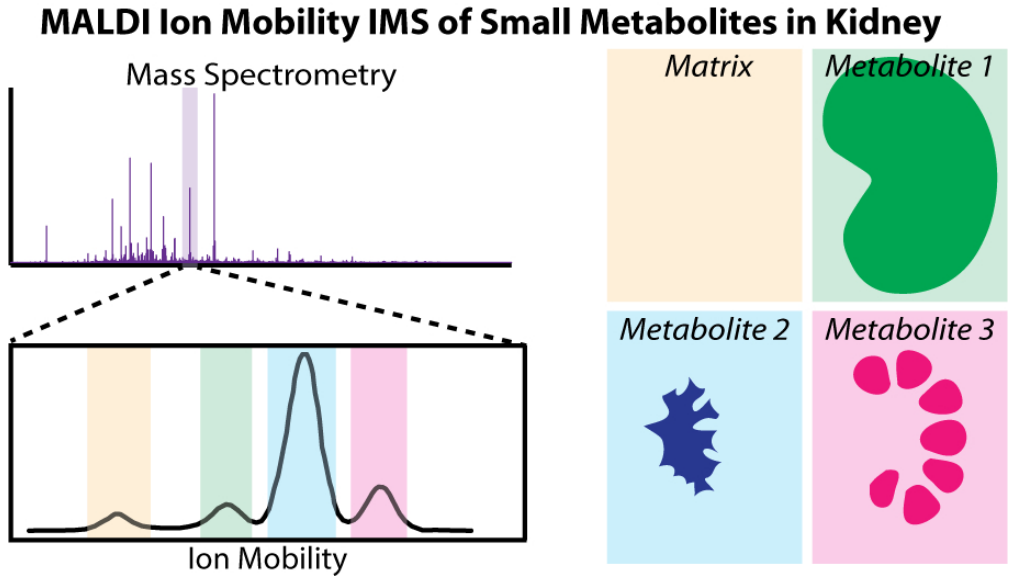
MALDI Ion Mobility IMS of Small Metabolites in Kidney
Mass Spectrometry
Ion Mobility
Matrix
Metabolite 1
Metabolite 2
Metabolite 3

TOC Image

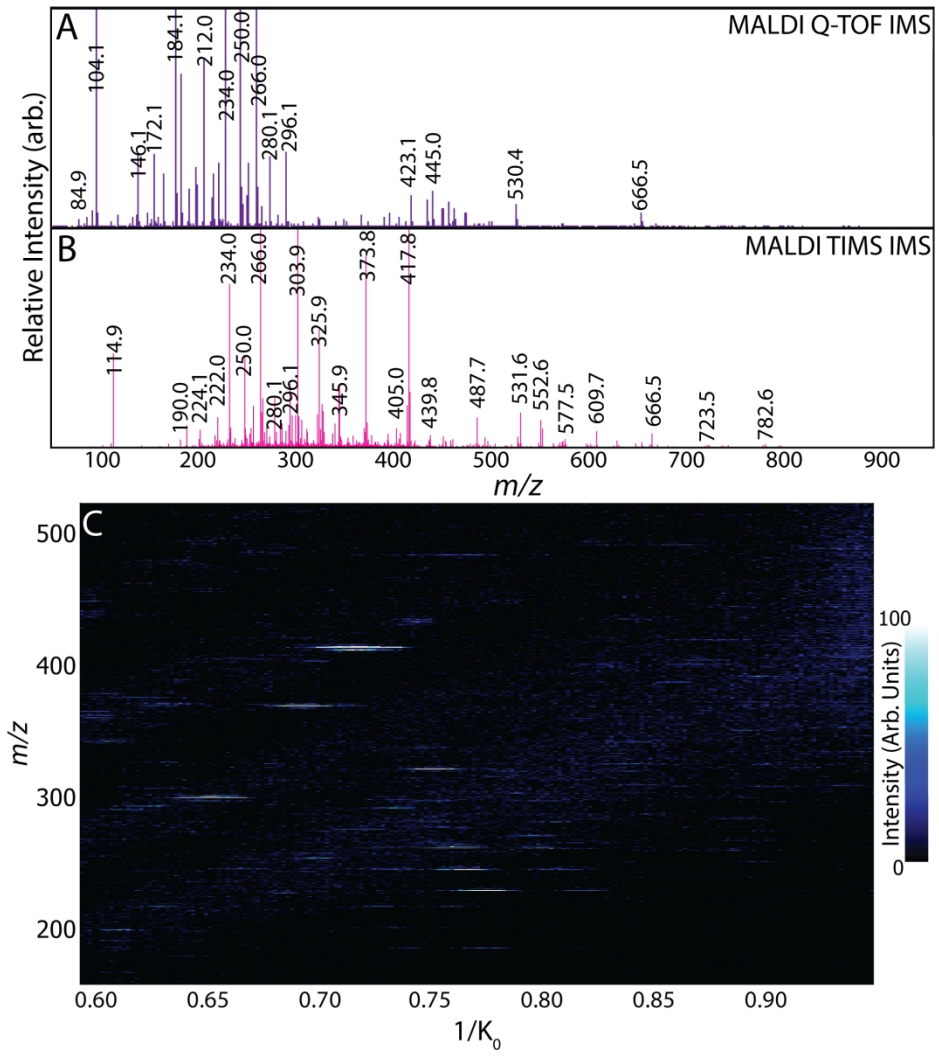

Figure 1: Average mass spectra of chemical features detect-ed within the human kidney in qTOF-only mode (A) and with TIMS enabled (B). Hundreds of chemical features are detected in both modes, but TIMS increases the number of detectable ions with the additional ion mobility component as seen in the mass spectra (B) and gel view image (C). The addition of TIMS separation reduces the detectability of ions below an m/z value of 150.

.1.5 mm

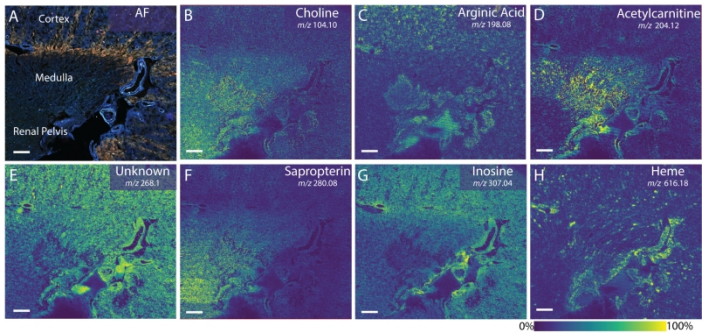

Figure 2: Selected ion images of small metabolites at 20 μm pixel size in comparison to autofluorescence (AF) microscopy (A), showing the spatial and size diversity of the detectable analytes (B-H). Each metabolite localizes to different regions within the kidney, such as the cortex, medulla, and renal pelvis. The selected ion images demonstrate our molecular cover-age from smaller m/z values (B) to larger values (H) with many ions detected between those values (C-G). Scale bars are 1.5 mm.

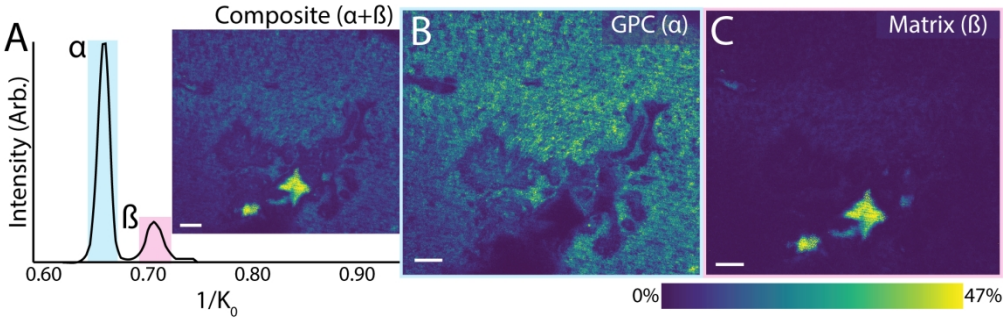

Figure 3: Ion mobility analysis can separate MALDI matrix ions from metabolite signals, increasing specificity of metab-olite imaging. Composite image (A inset) encompasses the distribution of an isobaric matrix and metabolite ion pair that can be separated in ion mobility space (A). Separate ion images of glycerophosphocholine (GPC) (m/z 258.1067, 0.677 ppm error, B) and the matrix (C) ions with detectable distributions outside and inside the kidney, respectively. Scale bars are 1.5 mm. For comparison, the corresponding autofluorescence image (Figure 2A).

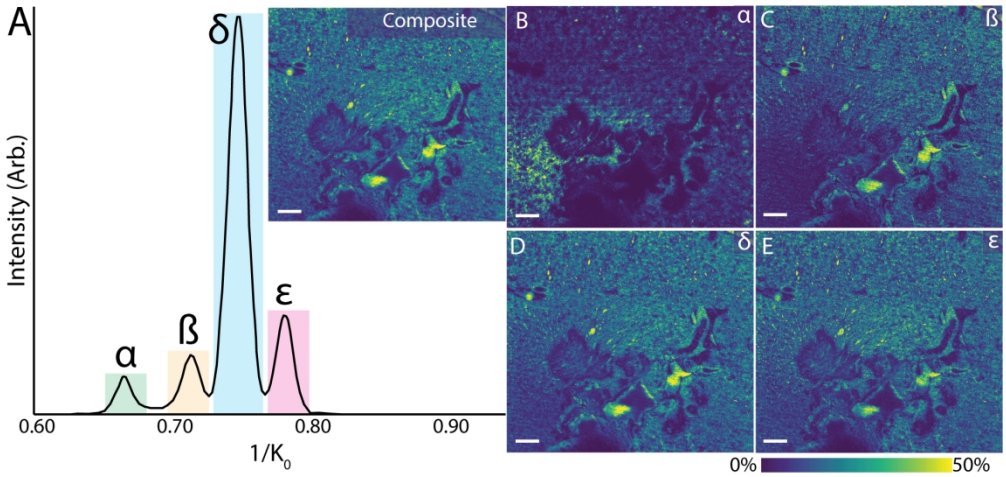

Figure 4: Ion mobility separations enable visualization of metabolite isobars/isomers increasing the peak capacity of MALDI IMS. Composite image (A inset, m/z 267.956) of four components separated within the ion mobility dimension (A). Each component can be separately visualized with the first component localizing to the renal pelvis (B) and the other three detected through the entire kidney section (C-E). Scale bars are 1.5 mm.